Exp Biomed Res 2024; 7(4): 197-207 **https://doi.org/ 10.30714/j-ebr.2024.224**

Experimental Biomedical Research *Original article*

Evaluation of photostability, cellular uptake, photochemical mechanism, and photodynamic efficacy of rose bengal-incorporated mesoporous silica nanoparticles

Tuğçe Mutlu[1], Mustafa Kemal Ruhi[1,*]

[1]*Institute of Biomedical Engineering, Boğaziçi University, İstanbul, Türkiye*

ABSTRACT

Aim: Rose bengal is a xanthene dye approved by the Food and Drug Administration for determining liver function and some ophthalmologic applications. Research has shown that rose bengal can also be used as an anti-cancer photodynamic therapy agent. However, its hydrophilic tendency and low half-life limit its accumulation in tumor tissue. The purpose of this study was to incorporate rose bengal with mesoporous silica nanoparticles and to conduct comprehensive analyses to investigate the synthesized nanoconjugates in terms of photostability, cellular uptake, and photodynamic therapy efficacy.

Methods: Rose bengal was incorporated into mesoporous silica nanoparticles and tested on the A-549 lung cancer cell line to evaluate its photostability, cellular uptake, photochemical mechanism, and photodynamic therapy efficacy. A 530 nm LED light source set to 100 mW/cm^2 was used to irradiate the samples.

Results: The 1,3-Diphenylisobenzofuran (DPBF) assay results demonstrated that the irradiation of rose bengal-loaded mesoporous silica nanoparticles initiated more DPBF degradation than free rose bengal (76% and 18% DPBF degradation in 5 minutes of irradiation, respectively), which indicates that the incorporation with MSN increases the photodynamic activity of the photosensitizer. Sodium azide assay showed that the photodynamic therapy effect was primarily through singlet oxygen production because the presence of sodium azide inhibited cell killing by around 50%. Additionally, the photostability of rose bengal was enhanced when loaded into the mesoporous silica matrix. However, the cellular uptake did not show a significant change (P<0.54).

Conclusions: The results show that incorporating rose bengal with mesoporous silica increases its efficacy as a photodynamic therapy agent and overcomes the limits of this dye as a photosensitizing agent. Although the cellular uptake did not change, it should be kept in mind that these experiments were conducted on an *in vitro* model, and the actual effect of this drug delivery strategy would be revealed under *in vivo* conditions, where circulation and extravasation take place.

Key words: Cancer treatment, photodynamic therapy, rose bengal, mesoporous silica nanoparticles.

* *Mustafa Kemal Ruhi*

Institute of Biomedical Engineering, Boğaziçi University, İstanbul, Türkiye

E-mail: kemal.ruhi@bogazici.edu.tr

Received: 2024-06-10 / Revisisons: 2024-07-05

Accepted: 2024-07-14 / Published: 2024-09-30

1. Introduction

Photodynamic therapy (PDT) is a cancer treatment method that relies on the production of cytotoxic reactive oxygen species (ROS) in tumor tissue via the excitation of photosensitive molecules (photosensitizers (PS)) by light (500-800 nm) [1-3]. This minimally invasive method

is advantageous over conventional treatment methods due to its high selectivity and lower side effects [3]. The photosensitizer is a crucial component of PDT. An ideal photosensitizer should create high cytotoxicity upon excitation by light and be selective to tumor tissue [4, 5]. The selectivity of the photosensitizers either happens naturally due to the enhanced permeability and retention (EPR) effect or is achieved by using active targeting strategies, such as monoclonal antibodies [6, 7]. Rose bengal (RB) is a U.S. Food and Drug Administration-approved xanthene dye used in PDT research as a photosensitizer due to its high ROS production capacity [8-10]. RB is hydrophilic, which is an advantage for its systemic administration. However, this property of RB hinders RB molecules from crossing hydrophobic cell membranes. Additionally, the short half-life of RB causes the molecules to degrade before staying in circulation long enough to accumulate in tumor tissue due to EPR [11]. To overcome this problem, drug delivery approaches, such as incorporating PSs into liposomes or nanoparticles, can be considered.

Mesoporous silica nanoparticles (MSN) are easy to synthesize and advantageous for drug loading due to their high surface area and biocompatibility [12]. Additionally, these nanoparticles are optically transparent, which is ideal for light-based applications. Furthermore, it has been shown that incorporation with MSN may increase the singlet oxygen quantum yield of the photosensitizers [13-15]. There are studies in the literature that consider MSN to be a delivery vehicle for RB. A theoretical study by Estevao et al. demonstrated that RB-loaded MSNs can increase $^1O_2$ production efficiency by preventing aggregation [16]. According to another study of the same research group, the optimized nanoconjugate, 4% RB-loaded MSNs reduced cell proliferation of melanoma cells (SK-MEL-28) [17]. Additionally, the authors showed that MSNs protect against photodegradation by creating a shielding effect for RB. Zhan et al. functionalized pH-responsive MSNs with Fe_3O_4 and utilized them for RB delivery [18]. The analyses on the cellular uptake, drug release, and concentration-dependent apoptosis rates on B16 mouse melanoma cells showed that the treatment with the developed nanoconjugates provided higher rates of apoptosis on B16 cells compared to free RB with minimal dark toxicity. Additionally, the study revealed that RB-loaded magnetic MSNs responded to the pH of endosomes and were rapidly released after endocytosis, which increased the drug concentration in the target area, yielding high cellular uptake. Despite these and other efforts, to the authors' knowledge, there is no comprehensive study in the literature that evaluates RB-incorporated MSNs (RB-MSNs) in terms of photostability, cellular uptake, photochemical mechanism, and PDT efficacy.

Our research aims to fill this gap by investigating the efficiency of RB-loaded MSNs as a PDT agent on the A-549 lung cancer cell line. According to the results of our study, the incorporation of RB molecules with MSN significantly increased their stability and singlet oxygen production. The primary mechanism of action of the new conjugates was Type II reaction-mediated, and the cellular uptake of MSN-RBs was not significantly different from the free RB.

2. Materials and metods

2.1. Synthesis of the MSNs: Ammonium-hydroxide (NH_4OH), cetyltrimethylammonium-bromide (CTAB), hydrochloric acid (HCl), tetraethyl-orthosilicate (TEOS), (3-Aminopropyl) triethoxysilane (APTES), RB and ethanol were obtained from Sigma-Aldrich.

MSNs were synthesized as described previously [19]. Briefly, 7.5 ml of distilled water and 1.057 ml of NH_4OH were mixed using a magnetic stirrer. The mixture was then completed to 30 ml by adding 21.44 ml of distilled water and remixed at 500 rpm and 40°C. Subsequently, 0.058 g CTAB was added to the mixture and allowed to dissolve. 118 µl TEOS and 482 µl ethanol were gradually added to the mixture, the temperature was raised to 60°C, and the mixture was stirred for two hours to precipitate the nanoparticles. After 2 hours, the nanoparticle solution was washed three times with ethanol using a centrifuge and a sonicator. The precipitated nanoparticles were dissolved in 20 ml ethanol, and 20 µl HCL was added. The mixture was then stirred at 500 rpm and 60°C for 3 hours. Finally, the MSNs were washed three times with ethanol.

2.2. Amino-Functionalization of MSNs using APTES: APTES is a chemical widely utilized in biology and chemistry, particularly for the surface modification and functionalization of silica-based nanoparticles like MSNs. When APTES is added to the MSN solution, it forms a covalent bond with the (-Si-OH) silanol groups on the silica surface, resulting in amino groups covering the MSNs' surface. This surface modification method improves the nanoparticle's stability and prevents aggregation of incorporated molecules in MSN pores, ensuring uniform dispersion [20]. In our study, MSNs were dissolved in 15 ml of ethanol, and 12 µl of APTES was slowly added to MSNs. The mixture was stirred in the magnetic stirrer at 500 rpm at room temperature for 24 hours. The mixture was then washed three times with ethanol.

2.3. Incorporation of RB into MSNs: APTES-functionalized MSNs were dissolved in 15 ml of ethanol and mixed with 3 mg of RB. The mixture was stirred at 500 rpm and at room temperature for 24 hours. The synthesized nanoparticles were then washed three times with ethanol, dissolved in distilled water, and kept in the freezer for use in future experiments.

2.4. Characterization of Nanoparticles: A standard curve was generated by measuring the absorbance of 20-200 µg/ml RB at 570 nm using the UV–Vis spectrophotometer to determine the RB amount in synthesized RB-MSNs. The absorption spectra of the nanoparticles were obtained using a Nanodrop 2000c UV–Vis spectrophotometer. A Scanning Electron Microscope (SEM) was utilized to determine the morphology of synthesized nanoparticles. Before imaging the nanoparticles, approximately 15 mg of MSNs were dissolved in 1.5 ml ethanol, and a homogeneous distribution was obtained using a sonicator. Subsequently, a drop of dissolved MSN was placed on the SEM templates, and images were taken. The size distribution was determined by the dynamic light scattering (DLS) technique, which relies on examining the light intensities caused by the movement and collision of molecules, known as Brownian motion [21]. Before DLS analysis, the synthesized MSNs were kept in a 60°C oven for 24 hours, and the number of synthesized MSNs was quantified using a precision weighing instrument. Approximately 15 mg of synthesized MSNs were dissolved with 1.5 ml ethanol, and the content was sonicated for homogenization and to prevent aggregation before DLS analysis.

2.5. Cell Culturing and Dark Toxicity Experiments: The A-549 lung cancer cells were cultured in Dulbecco's Modified Eagle Medium (DMEM) supplemented with 10% Fetal-Bovine Serum (FBS) and 1% Penicillin-Streptomycin. The cells were maintained in a 37°C incubator that contain 5% CO_2. The medium was changed every three days until the A-549 cell line achieved 80%-90% confluency and detached

from the flasks using Trypsin-EDTA for plating or passaging. Dark toxicity experiments were performed to evaluate the toxicity of RB-MSNs on A-549 cells without light irradiation. Cells were seeded in 96-well plates at 10,000 cells/well cell density, and plates were incubated for 24 hours before being incubated with 5, 10, 25, 50, 100, 250, 500, 750, and 1,000 μg/ml of RB-MSNs. After 2 hours of incubation, the RB-MSN-containing medium was removed, and the wells were washed three times with phosphate-buffered saline (PBS). The medium was then refreshed, and the plates were incubated for another 24 hours. For MTT analysis, the medium was removed from the wells and replaced with a new solution containing 10% MTT and 90% medium. Following 2 hours of incubation, the MTT solutions in the wells were removed and replaced with 100 μl DMSO. After incubation at room temperature on a shaker for 15 minutes, absorbance at 570 nm was determined using a microplate reader.

2.6. PDT Experiments: For PDT experiments, cells were seeded into wells of 96-well plates at 10,000 cells/well cell density. After 24 hours of incubation, the medium was replaced with RB-MSN solution at a concentration determined after the dark toxicity experiment. RB-MSNs were removed from the wells after 2 hours of incubation. Wells were washed with PBS, and a fresh medium was added to them. A 530 nm LED light source (Thorlabs M530L4) was set to 100 mW/cm^2 to irradiate groups (except no light controls) for 1, 5, 10, and 20 minutes. After 24 hours of incubation, the MTT assay was performed as described above.

2.7. Cellular Uptake Experiments: The uptake of free RB and RB-MSNs by the cells was measured as previously described (22). Briefly, cells were seeded into wells of a 6-well plate (1.5x10^5 cell/well) and incubated for 24 hours. Free RB and RB-MSN concentrations were added to the wells at previously determined concentrations and incubated for 2 hours. After 2 hours of incubation, cells were detached from the surface using trypsin-EDTA. Cells were placed in 15 ml falcon tubes and counted. Subsequently, cells were centrifuged at 1,000 rpm for 5 minutes and then gently washed with PBS. Each falcon tube was filled with 500 μl of 90% acetone to extract RB from cells. Finally, the supernatants were transferred to a 96-well plate, and the absorption values were determined using an absorbance plate reader at 570 nm. The determined absorption values were compared with a previously sketched standard curve with the linear equation:

$y = 0.0036x + 0.0962$, $R^2 = 0.9979$

where x = supernatant average absorbance and y = supernatant molarity.

The following equation was used to find RB contained in 1 μl of supernatant.

$$q = y.\frac{M_{RB}}{10^6}$$

where q = RB quantity in 1 μl of supernatant and M_{RB} = molar weight of RB.

Since the volume of the solution was 500 μl for each tube, the result was multiplied by 500. Finally, the amount of RB absorbed by a single cell was calculated by dividing the results for each tube by the corresponding number of cells. Two independent repeats were conducted.

2.8. Assessing the Role of Singlet Oxygen in Cellular Toxicity: Sodium azide is known as a singlet oxygen quencher. Therefore, it can be used to evaluate the dominant mechanism in PDT applications. In this analysis, inhibition of cell death in the presence of sodium azide would show that the cytotoxicity is mainly due to singlet oxygen produced by Type II reactions during PDT (23, 24).

The reaction between sodium azide (NaN3) and singlet oxygen ($^1O_2$) is as follows:

$NaN_3 + {}^1O_2 \rightarrow Na^+ + N^{-3} + O_2$.

First, a preliminary experiment was conducted to show that our sodium azide concentration does not cause any toxicity in the A-549 cells. Briefly, cells were incubated with 50 mM sodium azide for 2 hours, and an MTT assay was performed. The cells were then plated and treated as follows:

No treatment

RB-MSNs and light (530 nm, 20 minutes, 100 mW/cm^2)

RB-MSNs and light + sodium azide (530 nm, 20 minutes, 100 mW/cm^2).

2.9. Quantification of ROS Production Using DPBF Assay: The singlet oxygen production of free RB and RB-MSNs was compared using a 1,3-Diphenylisobenzofuran (DPBF) assay (25). In this method, the PDT agents are incubated with DPBF and irradiated with light that can excite the PDT agents. The produced singlet oxygen molecules during irradiation rapidly interact with DPBF, which causes a decrease in the absorbance peak of DPBF at 420 nm. Therefore, the rate of decline in this peak can be correlated with the singlet oxygen production of the PDT agents. In our study, RB and RB-MSN concentrations previously determined by the dark toxicity experiments were separately incubated with 10 mM DPBF. The absorbance values following 0, 1, 5, 10, and 20 minutes of irradiation (530 nm, 100 mW/cm^2) were determined using the UV-visible spectrophotometer at 420 nm. Two independent repeats were conducted.

2.10. Analysis of Photodynamic Stability: To compare the photostability of free RB and RB-MSNs, their previously determined concentrations were prepared in falcon tubes and kept at ambient temperature and light for 14 days. The absorption peaks of free RB and RB-MSNs at 550 nm were obtained and compared at 0, 3, 7, and 14 days.

2.11. Statistical Analysis: The data was compared using the Student's t-test (if two groups are compared) or ANOVA (if more than two groups are compared) after demonstrating that the groups show a normal distribution. ANOVA was followed by Tukey's multiple comparison test to compare the individual groups with each other statistically. The significance level will be taken as 5% (P<0.05) and marked using a (*) symbol in the graphs. All experiments were repeated at least three times if otherwise specified.

3. Results

3.1. Characterization of the Synthesized Nanoparticles: As shown in Figure 1a, the synthesized MSNs reveal a uniform spherical morphology, and their sizes are similar to the results obtained from the DLS experiment, where the hydrodynamic diameters of MSNs were calculated as 60-70nm (Figure 1b, Polydispersity Index (PDI): 0.211±0.071). The results show that uniform MSNs could be successfully synthesized.

3.2. Dark Toxicity Experiments: As shown in Figure 2, RB-MSN was significantly toxic at 1,000 μg/ml on A-549 cells. Therefore, the highest non-toxic concentration of RB-MSN, 750 μg/ml, was selected as the concentration for subsequent studies.

3.3. Determination of RB Content in RB-MSNs and Comparison of the Dark Toxicities of Free RB and MSN-incorporated RB: The standard curve generated by acquiring the absorbance of 20-200 μg/ml RB at 570nm, shown in Supplementary Figure 1, was used to determine the RB amount in synthesized RB-MSNs. According to the linear equation derived from this curve (see subsection 2.7), RB concentration in 750 μg/ml was calculated as 49.25 μg/ml. The comparison of the absorption spectra of these concentrations of free RB and

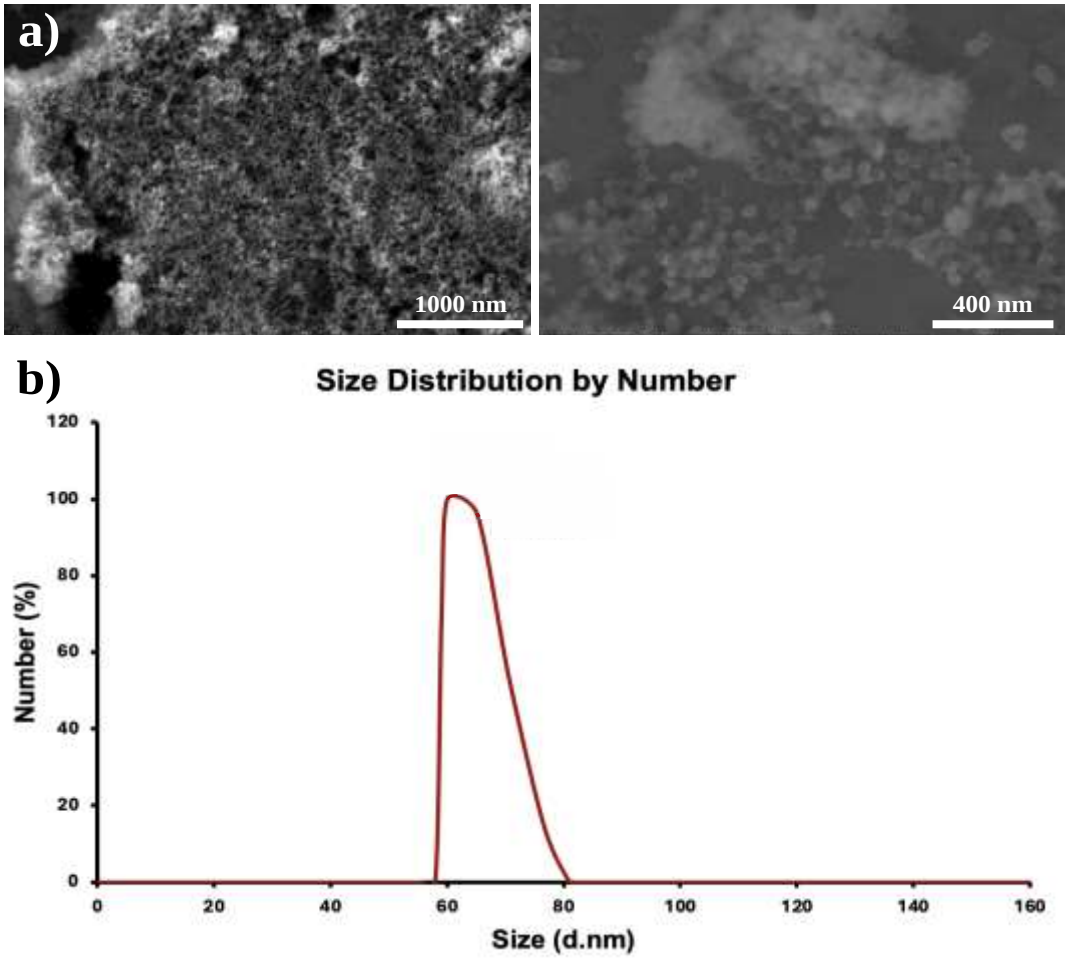

Figure 1. a) SEM images of MSNs. **b)** DLS analysis of MSNs.

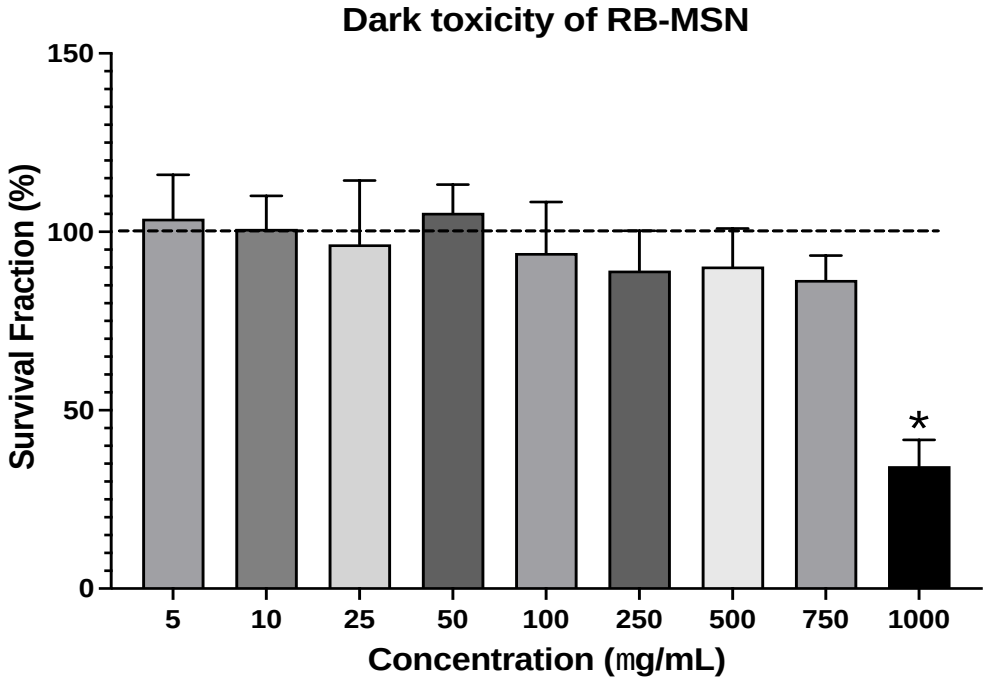

Figure 2. Survival fraction of A-549 cells with increasing RB-MSN concentration. Data of each group were normalized to respective no-treatment controls indicated by the dashed line. The group that is significantly different from no treatment was labeled by "*" ($P < 0.05$).

RB-MSNs is shown in Supplementary Figure 2. Similar absorption values confirm that the RB content of 750 μg/ml of RB-MSN is around 49.25 μg/ml.

3.4. PDT Experiments: The results of the PDT experiment have shown that the application of light in the presence of RB-MSN caused a significant decrease in normalized survival of A-549 cells compared to the control groups (Figure 3). The highest reduction in cell survival, 72%, was achieved with 20 minutes of irradiation. However, the PDT groups were not significantly different from each other.

3.5. Assessment of the Primary Mechanism of Action of PDT: The preliminary experiment results show that 50 mM sodium azide does not cause any toxicity in cells (Supplementary Figure 3). As shown in Figure 4, the results of the subsequent experiment showed that RB-MSNs-mediated PDT decreased the survival fraction by approximately 62% in the absence of sodium azide. In contrast, the same treatment could reduce the survival fraction by 13% in the presence of sodium azide. This shows that quenching singlet oxygen using sodium azide significantly decreases the RB-MSNs-mediated PDT efficacy.

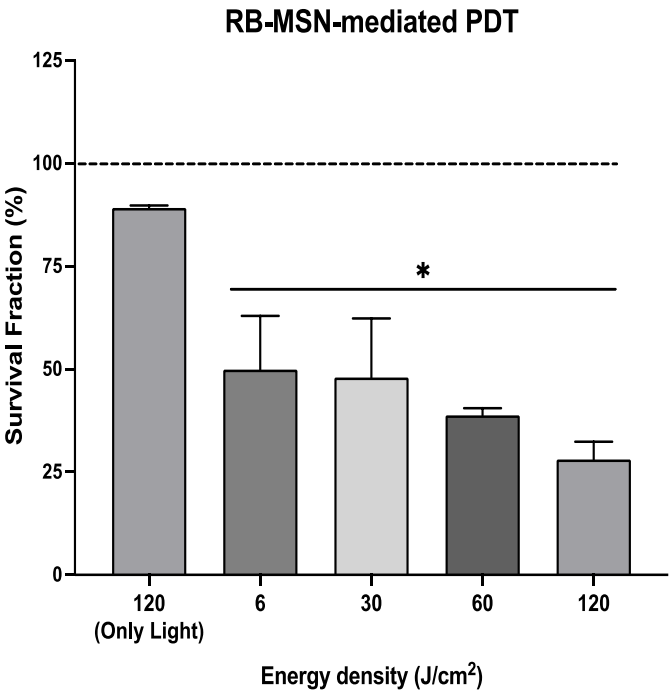

Figure 3. Survival fraction of A-549 cells incubated with RB-MSN and irradiated with given energy densities. Data of each group were normalized to respective no-treatment controls indicated by the dashed line. Groups that are significantly different from no treatment were labeled by "*" ($P < 0.05$).

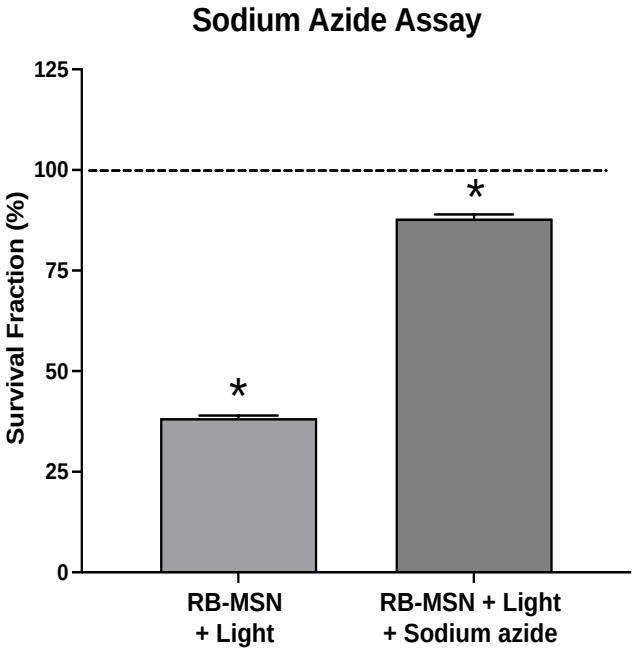

Figure 4. Survival fraction of A-549 cells after PDT in the absence and presence of 50 mM sodium azide. Data of each group were normalized to respective no-treatment controls indicated by the dashed line. Groups that are significantly different from no treatment were labeled by "*" ($P < 0.05$).

3.6. Comparison of the cellular uptake of free RB and RB-MSN: The graph shown in Figure 5 reveals that the cellular uptake of RB-MSNs was slightly less than free RB. However, the difference was not statistically significantly different. This result suggests that the incorporation of RB molecules into MSN negatively affected their uptake by A-549 cells.

3.7. Comparison of the Singlet Oxygen Production of Free RB and RB-MSN: The comparison of singlet oxygen production of free RB and RB-MSN was made using the DPBF assay. Figure 6 shows that the singlet oxygen

production of MSN-incorporated RBs was higher than free RB, consistent with the literature [13-15].

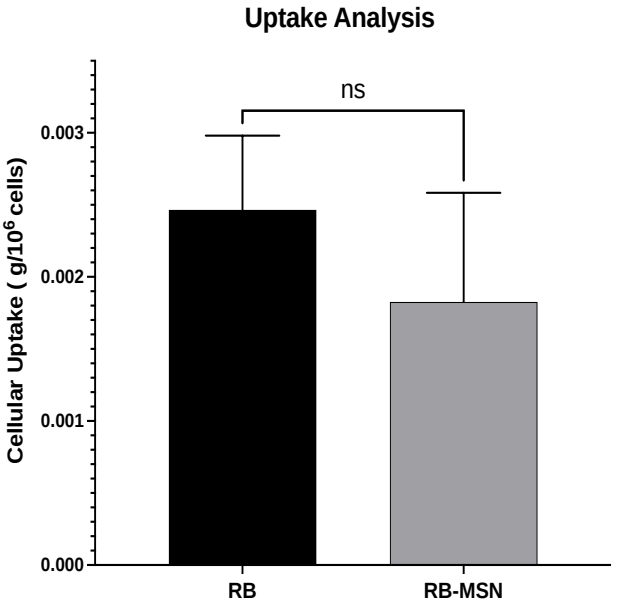

Figure 5. Comparison of cellular uptake of free RB and RB-MSN. ns: Not significant.

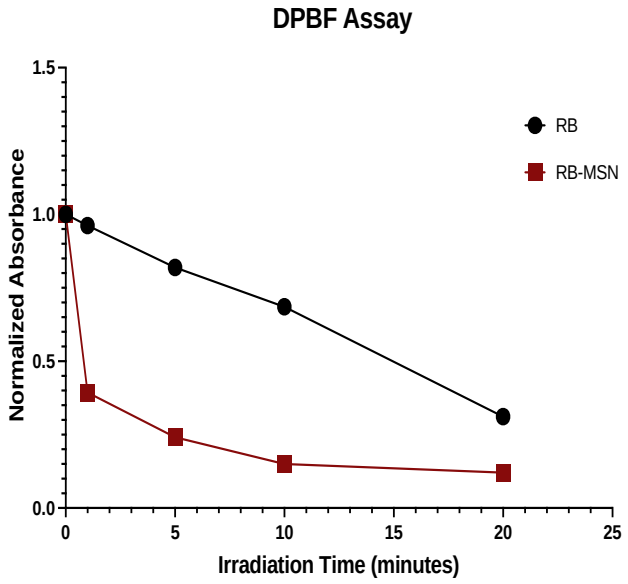

Figure 6. The decrease in absorption peak of DPBF after irradiation in the presence of RB (black/round, 49.25 μg/ml) and RB-MSN (red/square, 750.00 μg/ml).

3.8. Comparison of the Photostability of Free RB and RB-MSN: The curve shown in Figure 7a reveals that the absorbance of RB at 550 nm decreased continuously starting from the beginning of the experiment. The graph shown in panel c of the same figure shows that this decrease is statistically significant between the 1st and 14th days of the experiment. On the other hand, the absorbance of RB-loaded MSNs at 550 nm did not significantly change (Figure 7c).

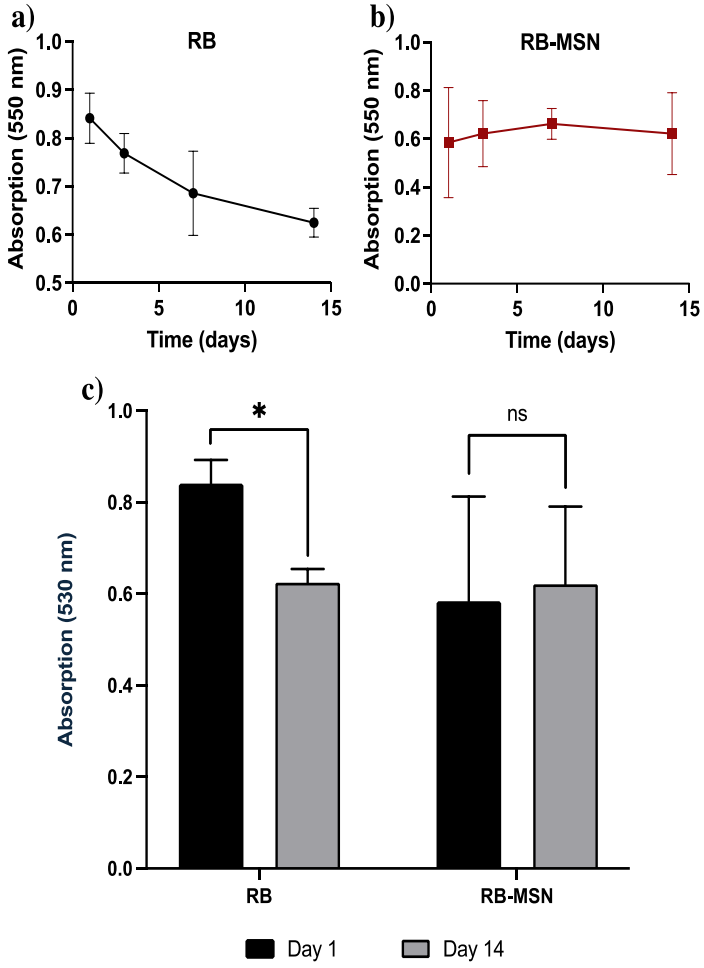

Figure 7. Photostability analysis results. a) Change in 49.25 μg/ml free RB absorbance at 550 nm. b) Change in 750.00 μg/ml RB-MSN absorbance at 550 nm. c) Comparison and statistical analysis of change in absorbance of RB (black/round) and RB-MSN (red/square) between Day 1 and Day 14. ns: Not significant.

4. Discussion

The effectiveness of PDT primarily depends on the accumulation of photosensitizer molecules in the tumor tissue and their successful stimulation by light in that area. Therefore, the photosensitizer molecules must reach the target tissue without self-aggregating or degrading within the body. Drug delivery methods such as MSN can protect photosensitizer molecules from degradation thanks to their pores, prevent aggregation, and maintain their photodynamic activity in preclinical and clinical applications. The primary aim of this study was to evaluate the PDT efficacy of MSN-incorporated RB on an *in vitro* lung cancer model. Our results demonstrated that incorporation with MSN increased RB's PDT efficacy and photostability. Although we hypothesized that the cellular uptake of hydrophilic RB would increase by their incorporation with MSN, the results did not show such an effect (Figure 5). However, it should be kept in mind that these experiments were conducted on an *in vitro* model, and the real effect of this drug delivery strategy will be revealed in *in vivo* conditions, where circulation and extravasation occur. This study also revealed that incorporation with MSN did not change the primary mechanism of action of RB-mediated PDT because the mechanism was still based on singlet oxygen production (Figure 4). Furthermore, consistent with previous studies, MSN incorporation increased the singlet oxygen generation capacity of RBs, likely due to the decreased degradation and increased local concentrations of RB molecules in MSN (Figure 6). Despite these promising findings, our study was conducted on the monolayer culture of one cancer cell line. Therefore, additional studies are necessary to reveal the effectiveness of RB-MSN as a PDT agent. Future research should focus on investigating the efficacy of this method on *in vivo* models and modifying the nanoparticles to enhance the efficacy of the proposed treatment further suitably. Combining this method with traditional treatment approaches can also be explored to improve the overall therapeutic outcomes.

4.1. Conclusions

To sum up, this study aimed to comprehensively investigate successfully synthesized RB-MSN nanoparticles in terms of photostability, cellular uptake, photochemical mechanism and PDT efficacy. The results revealed that the incorporation of RB with MSN enhanced its properties as a PDT agent.

Acknowledgment: *We would like to thank Prof. Dr. Bora Garipcan for their valuable contributions.*

Funding: *This study was supported by the Turkish Council of Higher Education (YÖK) Research Universities Support Program (ADP) Grant Number 50002.*

Conflict of interest: *The authors declare that they have no conflict of interest.*

Ethical statement: *Since this study was conducted in a laboratory environment, no ethics committee decision was taken.*

References

[1] Dougherty TJ, Gomer CJ, Henderson BW, et al. Photodynamic therapy. J Natl Cancer Inst. 1998;90(12):889-905.

[2] Kessel D. Photodynamic therapy: from the beginning. Photodiagnosis Photodyn Ther. 2004;1(1):3-7.

[3] Agostinis P, Berg K, Cengel KA, et al. Photodynamic therapy of cancer: an update. CA Cancer J Clin. 2011;61(4):250-81.

[4] Castano AP, Demidova TN, Hamblin MR. Mechanisms in photodynamic therapy: part one-photosensitizers, photochemistry and cellular localization. Photodiagnosis Photodyn Ther. 2004;1(4):279-93.

[5] Allison RR, Downie GH, Cuenca R, et al. Photosensitizers in clinical PDT. Photodiagnosis Photodyn Ther. 2004;1(1):27-42.

[6] Maeda H. The enhanced permeability and retention (EPR) effect in tumor vasculature: the key role of tumor-selective macromolecular drug targeting. Adv Enzyme Regul. 2001;41:189-207.

[7] Siemann DW. The unique characteristics of tumor vasculature and preclinical evidence for its selective disruption by Tumor-Vascular Disrupting Agents. Cancer Treat Rev. 2011;37(1):63-74.

[8] Paczkowski J, Lamberts JJ, Paczkowska B, et al. Photophysical properties of rose bengal and its derivatives (XII). J Free Radic Biol Med. 1985;1(5-6):341-51.

[9] Bartusik-Aebisher D, Ozog L, Domka W, et al. Rose Bengal and Future Directions in Larynx Tumor Photodynamic Therapy. Photochem Photobiol. 2021;97(6):1445-52.

[10] Koevary SB. Selective toxicity of rose bengal to ovarian cancer cells in vitro. Int J Physiol Pathophysiol Pharmacol. 2012;4(2):99-107.

[11] Sara Demartis AO, Elisabetta Gavini, Paolo Giunchedi, Giovanna Rassu. Nanotechnology-based rose Bengal: A broad-spectrum biomedical tool. Dyes and Pigments. 2021;188(109236).

[12] Sztandera K, Gorzkiewicz M, Klajnert-Maculewicz B. Nanocarriers in photodynamic therapy-in vitro and in vivo studies. Wiley Interdiscip Rev Nanomed Nanobiotechnol. 2020;12(3):e1509.

[13] Priti P. Pednekar SCG, Kisan R. Jadhav, Vilasrao J. Kadam. Mesoporous silica nanoparticles: a promising multifunctional drug delivery system. In: Anton Ficai AMG, editor. Nanostructures for Cancer Therapy: Elsevier; 2017. p. 593-621.

[14] Singh AK, Hahn MA, Gutwein LG, et al. Multi-dye theranostic nanoparticle platform for bioimaging and cancer therapy. Int J Nanomedicine. 2012;7:2739-50.

[15] Mendoza C, Desert A, Khrouz L, et al. Heterogeneous singlet oxygen generation: in-operando visible light EPR spectroscopy. Environ Sci Pollut Res Int. 2021;28(20):25124-9.

[16] Martins Estevao B, Cucinotta F, Hioka N, et al. Rose Bengal incorporated in mesostructured silica nanoparticles: structural characterization, theoretical modeling and singlet oxygen delivery. Phys Chem Chem Phys. 2015;17(40):26804-12.

[17] Gianotti E, Martins Estevao B, Cucinotta F, et al. An efficient rose bengal based nanoplatform for photodynamic therapy. Chemistry. 2014;20(35):10921-5.

[18] Zhan J, Ma Z, Wang D, et al. Magnetic and pH dual-responsive mesoporous silica nanocomposites for effective and low-toxic photodynamic therapy. Int J Nanomedicine. 2017;12:2733-48.

[19] Lin YS, Haynes CL. Impacts of mesoporous silica nanoparticle size, pore ordering, and

pore integrity on hemolytic activity. J Am Chem Soc. 2010;132(13):4834-42.

[20] Wang Y, Sun Y, Wang J, et al. Charge-Reversal APTES-Modified Mesoporous Silica Nanoparticles with High Drug Loading and Release Controllability. ACS Appl Mater Interfaces. 2016;8(27):17166-75.

[21] Goldburg WI. Dynamic light scattering. American Journal of Physics. 1999;67(12):1152–60.

[22] Colasanti A, Kisslinger A, Quarto M, et al. Combined effects of radiotherapy and photodynamic therapy on an in vitro human prostate model. Acta Biochim Pol. 2004;51(4):1039-46.

[23] Tavares A, Dias SR, Carvalho CM, et al. Mechanisms of photodynamic inactivation of a gram-negative recombinant bioluminescent bacterium by cationic porphyrins. Photochem Photobiol Sci. 2011;10(10):1659-69.

[24] Hamblin MR. Potentiation of antimicrobial photodynamic inactivation by inorganic salts. Expert Rev Anti Infect Ther. 2017;15(11):1059-69.

[25] Entradas T, Waldron S, Volk M. The detection sensitivity of commonly used singlet oxygen probes in aqueous environments. J Photochem Photobiol B. 2020;204:111787.